The evolutionarily conserved residue A653 plays a key role in HERG channel closing

Svetlana Z. Stepanovic[1], Franck Potet[1], Christina I. Petersen[1], Jarrod A. Smith[2], Jens Meiler[2,3,4,5], Jeffrey R. Balser[1,6] and Sabina Kupershmidt[1,3]

Departments of [1]Anesthesiology, [3]Pharmacology, [4]Biomedical Informatics, [5]Chemistry and [6]Medicine, and [2]Center for Structural Biology, Vanderbilt University School of Medicine, Nashville, TN 37232, USA

Human *ether-a-go-go*-related gene (*HERG*) encodes the rapid, outwardly rectifying K^+ current I_{Kr} that is critical for repolarization of the cardiac action potential. Congenital *HERG* mutations or unintended pharmaceutical block of I_{Kr} can lead to life-threatening arrhythmias. Here, we assess the functional role of the alanine at position 653 (HERG-A653) that is highly conserved among evolutionarily divergent K^+ channels. HERG-A653 is close to the 'glycine hinge' implicated in K^+ channel opening, and is flanked by tyrosine 652 and phenylalanine 656, which contribute to the drug binding site. We substituted an array of seven (I, C, S, G, Y, V and T) amino acids at position 653 and expressed individual variants in heterologous systems to assess changes in gating and drug binding. Substitution of A653 resulted in negative shifts of the $V_{1/2}$ of activation ranging from −23.6 (A653S) to −62.5 (A653V) compared to −11.2 mV for wild-type (WT). Deactivation was also drastically altered: channels with A653I/C substitutions exhibited delayed deactivation in response to test potentials above the activation threshold, while A653S/G/Y/V/T failed to deactivate under those conditions and required hyperpolarization and prolonged holding potentials at −130 mV. While A653S/G/T/Y variants showed decreased sensitivity to the I_{Kr} inhibitor dofetilide, these changes could not be correlated with defects in channel closure. Homology modelling suggests that in the closed state, A653 forms tight contacts with several residues from the neighbouring subunit in the tetramer, playing a key role in S6 helix packing at the narrowest part of the vestibule. Our study suggests that A653 plays an important functional role in the outwardly rectifying gating behaviour of HERG, supporting channel closure at membrane potentials negative to the channel activation threshold.

(Received 18 November 2008; accepted after revision 31 March 2009; first published online 30 April 2009)
Corresponding author S. Kupershmidt: Department of Anesthesiology, 2213 Garland Ave, P-445 MRB4, Vanderbilt University School of Medicine, Nashville, TN 37232, USA. Email: sabina.kupershmidt@vanderbilt.edu

Abbreviations CHO, Chinese hamster ovary; GFP, green fluorescent protein; *HERG*, human *ether-a-go-go*-related gene; LQTS, long QT syndrome; PDB, protein data bank; WT, wild-type.

Potassium (K^+) channels can be grouped into several classes of multigene families that exhibit substantial structural diversity but also contain recognizable common features (Lu *et al.* 2001; Roden *et al.* 2002; Armstrong, 2003; Pischalnikova & Sokolova, 2009). Their structural diversity further expands when complex subunit interactions, as well as hetero- and homomeric assembly patterns are taken into account. Crystallographic data for the KcsA, MthK and KvAP bacterial channels, as well as for the mammalian *Shaker* family Kv1.2 channel, suggest a highly conserved structural scaffold for K^+ ion selectivity, gating mechanisms and voltage sensing (Doyle *et al.* 1998; Lu *et al.* 2001; Zhou *et al.* 2001; Jiang *et al.* 2002, 2003; Long *et al.* 2005*a*).

The rapid component of the cardiac delayed rectifier K^+ current, I_{Kr}, encoded by *HERG*, is an important contributor to repolarization of the cardiac action potential (Sanguinetti *et al.* 1995; Curran *et al.* 1995; Trudeau *et al.* 1995; Tseng, 2001). Numerous genetic mutations in *HERG* have been associated with the congenital long QT syndrome (LQTS), a cardiac disorder characterized by increased susceptibility to ventricular arrhythmias and sudden death (Roden & Spooner, 1999; Roden & Viswanathan, 2005). Suppression of I_{Kr} is also implicated in the aetiology of the acquired LQTS. In this case, the underlying mechanism is unintended block of the HERG channel by therapeutic agents (Roden & Viswanathan, 2005), especially when complicating factors,

 DOI: 10.1113/jphysiol.2008.166694

such as structural heart disease or electrolyte imbalance are also present (Choy *et al.* 1996; Armoundas *et al.* 2001; Etheridge *et al.* 2003).

At the resting membrane potential HERG channels are normally closed, in contrast to inward rectifier K^+ channels that regulate the cell membrane potential. Upon depolarization, HERG displays peculiar gating properties that combine channel opening and rapid inactivation, limiting the outward current. Upon repolarization, channels recover from inactivation more rapidly than they close (deactivate), evoking a large outward current that augments cellular repolarization (Smith *et al.* 1996). The majority of drugs that target HERG require the opening of the channel's intracellular gate for binding (Snyders & Chaudhary, 1996; Spector *et al.* 1996; Kiehn *et al.* 1996; Zou *et al.* 1997; Kamiya *et al.* 2006). Studies in voltage-gated K^+ channels implicate the so-called 'glycine-hinge' (Fig. 1) or the S4–S5 linker, in combination with the S6-COOH terminus region, in channel opening (Chen *et al.* 2001; Lu *et al.* 2001, 2002; Tristani-Firouzi *et al.* 2002; Decher *et al.* 2004; Long *et al.* 2005*a*,*b*). However, the exact position of the gate, and the mechanism of coupling between voltage sensing and opening and closing of the activation gate remain the subject of intense investigation for most voltage-gated ion channels.

The alanine (A) at position 653 in the S6 region of HERG (HERG-A653) is highly conserved across K^+ channel families and species with few exceptions (KcSA and KvAP, Fig. 1). The glycine hinge (Fig. 1), implicated in K^+ channel opening (Jiang *et al.* 2002; Magidovich & Yifrach, 2004; Ding *et al.* 2005), is five residues upstream of A653. In addition, HERG-A653 is bracketed by two key aromatic residues, Y652 and F656 that are key to high-affinity drug binding of HERG (Lees-Miller *et al.* 2000; Fernandez *et al.* 2004; Kamiya *et al.* 2006). Our current findings indicate that HERG-A653 also influences drug binding.

Our functional data in *Xenopus* oocytes and mammalian cells indicate that channel deactivation and closure at physiologically relevant potentials is critically dependent upon residue 653. Computational modelling suggests that the WT alanine at position 653 packs with hydrophobic residues F656, V659 and I655 from the adjacent subunit at the closest contact points between neighbouring S6 domains in the closed state. Thus, the evolutionarily conserved A653 residue plays an essential functional role in HERG closure.

Methods

Mutagenesis and channel expression in *Xenopus* oocytes and mammalian cells

Mutations were introduced in the *HERG* cDNA contained on plasmid pSP64T (Promega, Madison, WI, USA)

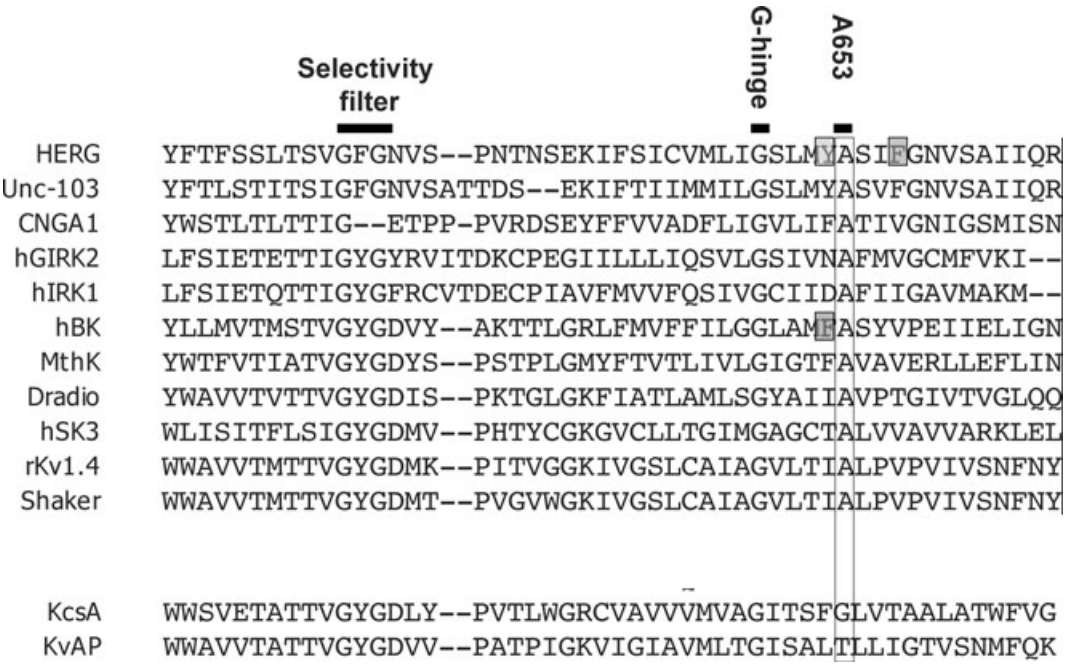

Figure 1. Amino acid alignment of the S6 transmembrane segments in HERG and twelve other K^+ channels

HERG-A653, a residue conserved in all channels except KcsA and KvAP is boxed. The positions of the selectivity filter and glycine hinge (G-hinge) are indicated by a black bar on the top, and other residues mentioned in the text are shaded.

using the Quick Change site-directed mutagenesis kit from Stratagene (La Jolla, CA, USA) and confirmed by sequencing the entire *HERG* cDNA. Constructs were linearized with *Eco*R I and RNA transcribed with SP6 RNA polymerase using the mMessage mMachine Kit from Ambion (Austin, TX, USA). *Xenopus laevis* oocytes were kindly provided by Dr Louis DeFelice's laboratory at Vanderbilt University and prepared as described previously (Adams & DeFelice, 2003) according to IACUC guidelines. Vanderbilt is fully accredited by the Association for Assessment and Accreditation of Laboratory Animal Care. Oocytes were injected on the same day with 50 ng cRNA/oocyte and stored at 18°C for 12–16 h in ND96 solution (96 mM NaCl, 2 mM KCl, 1 mM $MgCl_2$, 5 mM Hepes, pH 7.6) supplemented with 0.6 mM $CaCl_2$, 1 mM sodium pyruvate, 5% dialysed horse serum and 100 μg ml^{-1} streptomycin–tetracycline.

The *HERG* mutations were transferred to a mammalian expression vector, by transferring a 1.6 kb *Bst*X I and *Xho* I restriction enzyme fragment to the WT *HERG* backbone contained on pCGI (Kupershmidt *et al.* 2003), a bicistronic vector also expressing the green fluorescent protein (GFP). All plasmids were validated by sequencing. Chinese hamster ovary (CHO-K1) cells growing in 60 mm dishes were transfected with 3 μg of *HERG* (or *HERG* variant) cDNA contained on plasmid pCGI using FuGENE (Roche Applied Science).

Electrophysiology and drug application

The two-microelectrode voltage-clamp technique was used to record ionic currents with an Oocyte Clamp OC-725C (Warner Instruments). Currents were recorded at room temperature (RT) (22–24°C) 18–72 h after cRNA injection. Glass microelectrodes (borosilicate, thin wall with filament) were pulled using a Flaming–Brown micropipette puller P-87 (Sutter Instruments) to obtain resistances of 1–3 MΩ when filled with 3 M KCl. Currents were recorded in ND96 solution adjusted to pH 7.6. Drugs were applied by adding an appropriately concentrated stock solution to a premeasured bath volume. Drugs were prepared in acidified water for better dissolution and kept at −20°C for long-term storage, or at 4°C for short-term use.

Green fluorescent CHO cells were chosen for analysis, and HERG currents were recorded using the whole-cell patch clamp technique as described previously (Kupershmidt *et al.* 2003) using glass pipettes of 2–5 MΩ resistance. The standard intracellular (pipette) solution contained (in mM): 110 KCl, 10 Hepes, 5 K_4BAPTA, 5 K_2ATP, 1 $MgCl_2$, adjusted to pH 7.2 with KOH to yield a final intracellular K^+ concentration of 145. The extracellular (bath) solution contained (in mM): 140 NaCl, 5.4 KCl, 1 $MgCl_2$, 10 Hepes, 10 glucose, 2 $CaCl_2$, adjusted to pH 7.4 with NaOH. Patch-clamp measurements were performed at RT, 12–24 h post-transfection. Leak subtraction was not used.

Data analysis

Current recordings were acquired using Clampex 8.1 software. Clampfit 8.1 (Axon Instruments) and Origin 6.1 (Microcal Software) were used for data analysis. Data are presented as mean ± S.E.M., and statistical significance was tested using Student's independent *t* test. Differences were considered significant at $P < 0.05$, unless otherwise noted. The holding potential was −80 mV in oocytes and −130 mV in CHO cells.

Activation and inactivation curves were fitted to a Boltzmann function (continuous lines) of the form: $I = 1/[1 + \exp(V_t - V_{1/2})/\delta)]$, where $V_{1/2}$ is the half-activation potential and δ is the slope factor.

Deactivation time constants were obtained by fitting current traces to the standard bi-exponential curve according to the formula: $f(t) = A_f \exp(t/\tau_f) + A_s \exp(t/\tau_s) + C$. τ_f is the time constant of the fast component, τ_s is the time constant of the slow component, A_f and A_s are the relative amplitudes of the fast and slow components, and C is a constant.

Molecular modelling

Homology models of the HERG pore region in the open and closed states were constructed based upon the X-ray crystal structures of KvAP (protein data bank (PDB) entry: 1ORQ) and KcsA (PDB entry: 1K4C), respectively. We used the BCL::Align software to align the HERG sequence onto each template structure. Ten open- and closed-state homology models of the wild-type (WT) HERG monomer were then constructed using the loop-building mode in Rosetta (Rohl *et al.* 2004; Masetti *et al.* 2007). Residues corresponding to the 37 amino acid loop between S5 and the P-loop were removed (residues 574–609), as this region of the protein cannot be reliably modelled due to the absence of template coordinates. Tetramer models were generated by aligning the HERG monomer models onto the tetrameric crystal structure templates using UCSF Chimera software (Pettersen *et al.* 2004). At this stage, one copy each of the WT open- and closed-state tetramer model was modified to produce A653C, A653G, A653I, A653S, A653T, A653V and A653Y mutant tetramers. The WT and mutant tetramer models were then refined using several rounds of side chain repacking and gradient minimization in Rosetta, until the models converged in both energy and coordinate space. The lowest energy closed- and open-state models were then selected for further analysis. Additional details of the methodology used here

have been previously described elsewhere (Smith *et al.* 2007).

Results

The alanine at position 653 is critical for channel deactivation and closure

To investigate the role of the highly conserved alanine residue at position 653 in HERG gating, we assessed the functional effects of seven point mutations, chosen to introduce diverse structural elements at that position. All seven mutants, A653C/I/G/S/T/V and A653Y, were expressed and displayed measurable currents in *Xenopus* oocytes, leading us to conclude that membrane trafficking was not impeded in this system.

Uninjected oocytes were assessed for endogenous currents under the same voltage-clamp protocol in parallel experiments and recordings were made only if background currents were negligible. Currents elicited in response to a 'standard' voltage protocol are shown in Fig. 2*A*. Under these conditions, WT channels open at potentials above −50 mV and fully deactivate within 2 s when repolarized to −70 mV (Fig. 2*A*, WT). However, mutant channels deactivated more slowly (A653C and I) or showed little to no deactivation (A653S/G/Y/V/T, Fig. 2*A*) in response to pulses above −70 mV. They conduct inward current in response to more hyperpolarized potentials (bottom

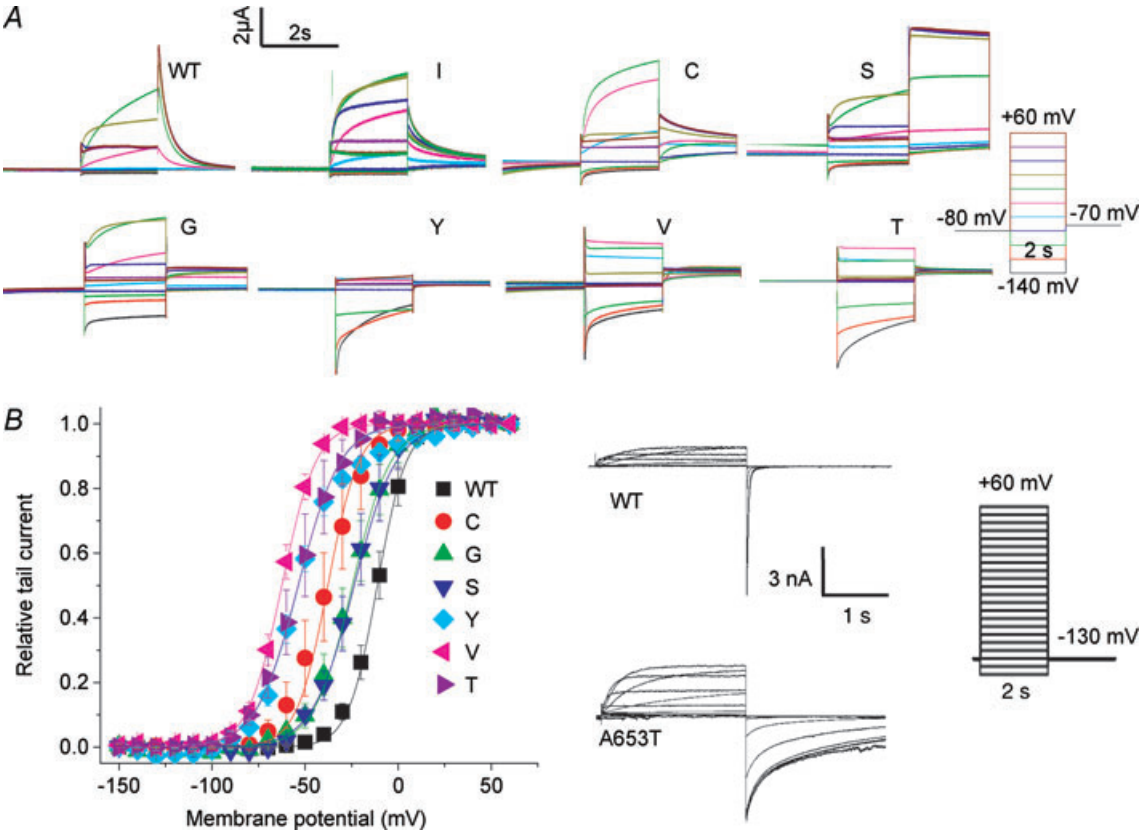

Figure 2. Functional effects of seven variants at HERG position 653
A, HERG currents in *Xenopus* oocytes were measured in response to the voltage protocol, shown on the right. A653C and A653I are closed at potentials negative to −60 mV and, when compared to WT, show slower but prominent deactivation upon hyperpolarization to −70 mV. A653S/G/Y/V/T show progressively greater defects in deactivation at −70 mV, as well as inward conduction at more negative potentials. *B*, activation curves for WT-HERG and A653 variants expressed in CHO cells. The half-activation potential was −11.2 ± 2.2 mV ($n = 6$) for WT, −23.6 ± 4.2 mV ($n = 6$) for A653S, −24.6 ± 3.9 mV ($n = 5$) for A653G, −37.8 ± 5.8 mV ($n = 6$) for A653C, −53.5 ± 1.5 mV ($n = 6$) for A653Y, −62.5 ± 1.6 mV ($n = 3$) for A653V and −53.7 ± 4.9 mV ($n = 4$) for A653T (in all cases, $P < 0.05$). A653I did not express current in CHO cells. Centre, representative raw current traces from CHO cells transfected with 3 μg WT-HERG or A653T cDNA. Far right, voltage protocol used for transfected CHO cells. Cells were held at −130 mV, and then stepped to test potentials between −150 and +60 mV in 10 mV increments for 2 s before repolarizing to −130 mV. The cells were held at −130 mV for 15 s before the next test pulse.

row, Fig. 2*A*). This indicated that the A653 variants are impaired at achieving the closed state at physiologically relevant potentials and that very negative potentials may be required to allow them to deactivate. To achieve this, we changed the holding potential to −130 mV.

To improve voltage control at these non-physiological test potentials, and to avoid possible endogenous background currents in *Xenopus* oocytes, we expressed the same variants in mammalian CHO cells for subsequent whole-cell patch-clamp analysis. As indicated by the voltage protocol in Fig. 2*B*, following voltage test steps ranging from −150 to +60 mV, we repolarized to −130 mV and recorded tail currents. The protocol also included a 15 s interval between test pulses to ensure complete closing of the channels and to allow us to construct activation curves for each mutant (Fig. 2*B*). Raw current traces for WT and a representative variant (A653T) elicited in response to this protocol are shown on the right. All mutant channels exhibit a pronounced leftward shift in voltage dependence of activation (Fig. 2*B*). The half-activation potential was −11.2 ± 2.2 mV ($n = 6$) for WT, −23.6 ± 4.2 mV ($n = 6$) for A653S, −24.6 ± 3.9 mV ($n = 5$) for A653G, −37.8 ± 5.8 mV ($n = 6$) for A653C, −53.5 ± 1.5 mV ($n = 6$) for A653Y, −53.7 ± 4.9 mV for A653T ($n = 4$) and −62.5 ± 1.6 mV ($n = 3$) for A653V ($P < 0.05$). Thus, the hyperpolarizing shift in $V_{1/2}$ between WT and mutants ranged from −12.4 (A653S) to −51.3 mV (A653V). For each variant, the activation curve exhibited steep voltage dependence, indicating that the S6 domain remains closely coupled with the voltage sensor. The hyperpolarizing shift in $V_{1/2}$ of activation, combined with the defects in channel deactivation, would result in inappropriate channel opening under physiologically relevant conditions. We were unable to collect data for A653I due to lack of currents expressed following multiple transfections of the mutant cDNA construct into CHO cells.

To describe channel deactivation in greater detail, we applied the following two-step protocol in *Xenopus* oocytes. Channels were depolarized for 500 ms to fully activate and inactivate all channels. We then applied a 2 s repolarizing pulse to −100 mV, during which WT channels quickly recover from inactivation and deactivate (see voltage protocol in Fig. 3*A*). We fitted deactivation traces to a standard bi-exponential curve and derived the slow (Fig. 3*A*) and fast (Fig. 3*B*) time constants of deactivation (see Methods). All but the A653I mutant exhibited a significant increase in the time constant for the slow component of deactivation, τ_s, compared to the WT (Fig. 3*A*). The τ_s (in ms) were 210 ± 52 for WT, 364 ± 100 for A653I, 552 ± 95 for A653C, 824 ± 154 for A653S, 1358 ± 95 for A653G, 1545 ± 139 for A653Y, 1158 ± 54 for A653V and 1380 ± 143 for A653T. The fast component of deactivation, τ_f, was significantly changed in A653C (128 ± 44 ms), A653S (131 ± 23 ms) and A653G (180 ± 13 ms) when compared to WT (32 ± 15 ms). Thus, we observed an overall slowing in deactivation time constant, which was especially pronounced for the slow component, and which is reflected in the deactivation impairment illustrated in Fig. 2*A*.

A653 variants do not affect inactivation properties

Next, we assessed how residue A653 impacts the voltage dependence of inactivation. For HERG, the steady-state inactivation is typically assessed using a 3-step protocol (see inset in Fig. 4*A*) (Smith *et al.* 1996). Currents that declined at the negative voltages because of significant closing of channels due to deactivation were corrected by extrapolation as described previously (Smith *et al.*

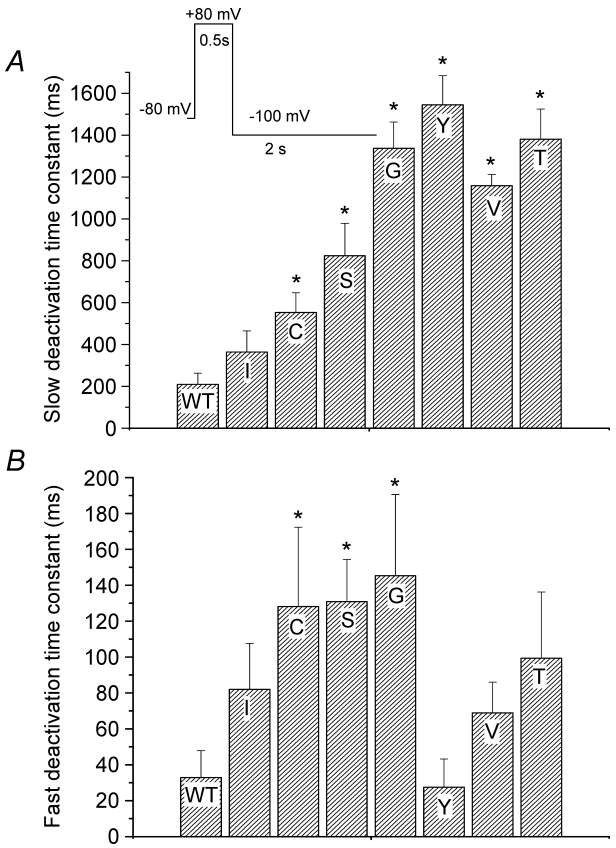

Figure 3. Variants at position 653 exhibit impaired deactivation
A, values (mean ± S.E.M.) were obtained by double exponential fits to deactivating current traces recorded at −100 mV (see Methods). Slow deactivation time constants (in ms), τ_s, were 210 ± 52 for WT, 364 ± 100 for A653I, 552 ± 95 for A653, 824 ± 154 for A653S, 1358 ± 95 for A653G, 1545 ± 139 for A653Y, 1158 ± 54 for A653V and 1380 ± 143 for A653T. All but A653I were significantly different from WT (*$P < 0.05$, $n = 3$–9). The voltage protocol is shown at the top. *B*, fast deactivation time constants, τ_f, were: 32 ± 15 for WT, 82 ± 25 for A653I, 128 ± 44 for A653C, 131 ± 23 for A653S, 180 ± 13 for A653G, 27 ± 15 for A653Y, 69 ± 17 for A653V and 99 ± 36 for A653T. A653C/S and G were significantly (*$P < 0.05$, $n = 3$–9) different from WT.

1996). Figure 4*A* shows normalized current plotted against the clamp potential during the second voltage step, and fitted to a Boltzmann function. The $V_{1/2}$ of steady-state inactivation was significantly altered in two mutants, A653Y (-64.9 ± 3.8 mV) and A653G (-26.7 ± 3.0 mV) *vs.* -41.2 ± 5.6 mV for WT ($P < 0.05$).

Residue 653 does not influence K^+ selectivity

To test whether the A653 mutations affect the K^+ selectivity of the HERG channel, we chose A653T as one of the most severely affected mutants and measured the effects of the amino acid change on reversal potential. There were no significant changes in the reversal potential between WT HERG (-86.0 ± 1.2, $n = 23$) and HERG-A653T (-87.1 ± 0.9 mV, $n = 26$), indicating that amino acid substitutions at residue 653 do not affect K^+ selectivity of HERG. In contrast, we found that the resting potential of oocytes expressing mutant channels differed significantly from those expressing WT channels (Fig. 4*B*). Given that K^+ selectivity is not altered in the mutants, the increased hyperpolarization of the oocyte resting potential in mutants most probably results from the hyperpolarizing shift in voltage dependence of activation evident in Fig. 2*B*.

Mutating HERG-A653 affects channel block by dofetilide

Given the location of the A653 residue between the Y652 and F656 residues, the putative receptor site for methanesulfonanilide drugs (Snyders & Chaudhary, 1996; Lees-Miller *et al.* 2000; Mitcheson *et al.* 2005; Kamiya *et al.* 2006), we tested whether the A653 mutations affect channel block by the prototypical HERG-inhibitor dofetilide. The onset of dofetilide block depends on channel opening and develops slowly with repeated pulsing. We therefore used a repetitive two-step protocol involving a 1 s depolarization to -20 mV, followed by a 3 s repolarization to -80 mV, for a total of 26 min where

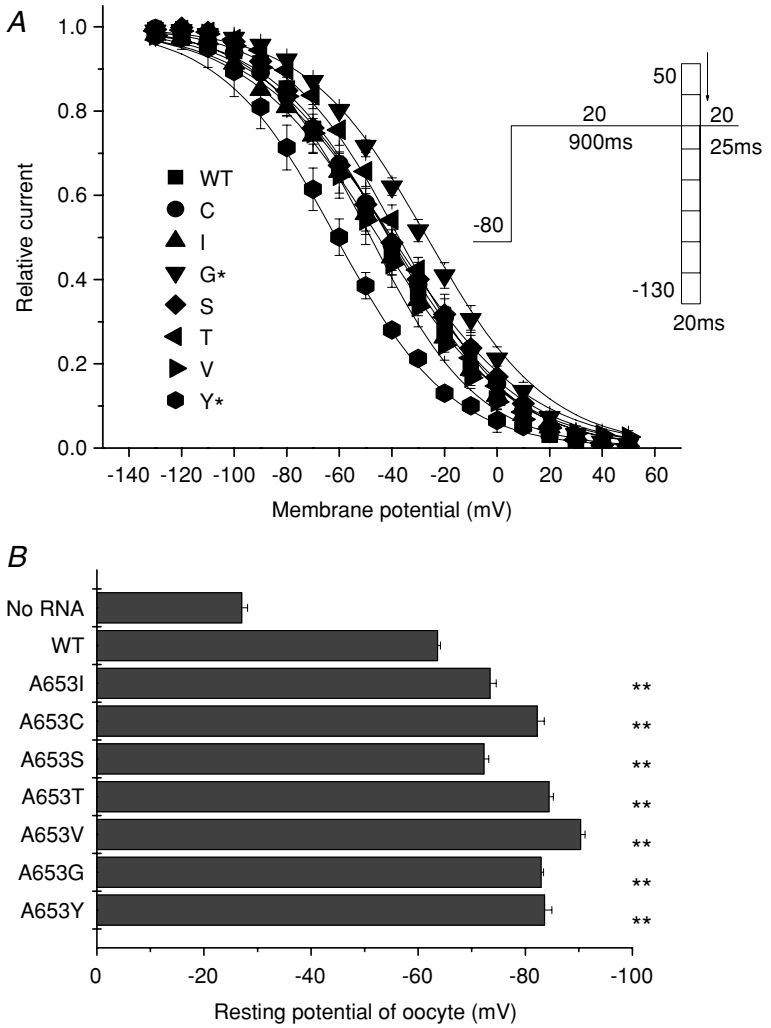

Figure 4. Inactivation properties of HERG-653 variants, and resting membrane potential of injected oocytes
A, steady-state inactivation was measured for WT and variants at position 653 using the voltage protocol shown in the inset. The $V_{1/2}$ of steady-state inactivation was -41.2 ± 5.6 for WT, -45.1 ± 3.1 for A653I, -40.8 ± 7.6 for A653C, -39.9 ± 5.0 for A653S, -26.7 ± 3.0 for A653G, -37.4 ± 3.5 for A653T, -48.1 ± 6.2 for A653V and -64.9 ± 3.8 for A653Y ($n = 5$–7); only A653Y and A653G differed significantly from WT (*$P < 0.05$). *B*, resting potential of *Xenopus* oocytes injected with WT and HERG-A653 variants ranged from -72 ± 0.9 to -90 ± 0.8 mV in the mutants *vs.* -63 ± 0.5 mV in WT); $n = 12$–76, **$P < 0.01$.

the first 2 min are recorded in the absence of dofetilide. We measured the total reduction in activating current magnitude expressed as fraction of the control current, as an index of dofetilide block.

Figure 5 shows the fraction of HERG current blocked in response to 1 μM dofetilide. We found one mutant (A653C) with slightly increased sensitivity to dofetilide, two mutants with sensitivity comparable to WT (A653I/V) and four mutants with significantly reduced sensitivity (A653S/G/T and Y). Even at saturating concentrations (10 μM), dofetilide block is reduced in A653T compared to WT (0.71 ± 0.09 *vs.* 0.92 ± 0.04) (Fig. 5, bottom). However, we discerned no correlation between the severity of the gating changes observed in Fig. 2 and drug sensitivity. We therefore conclude that the reduction in affinity observed with some of the A653 site variants is probably due to effects on the binding site rather than effects on gating.

Computational modelling suggests A653 anchors the narrowest part of the vestibule in the closed state

The molecular basis of the role of A653 in channel function was explored using homology modelling techniques. We examined the interactions of HERG residue 653 in 3-D homology models of open- and closed-state HERG for WT, as well as for the individual A653C/G/I/S/T/V/Y mutants. Figure 6 shows the WT and the A653T variants modelled in the closed state. The most striking finding was that, in the closed-state models, A653 occupies a position in the S6 helix which is in very close proximity to the S6 helix of an adjacent subunit (Fig. 6*A* and *B*). This proximity is lacking in the open state. Measuring inter-residue distances across the S6–S6 interface of two adjacent subunits confirms that, in the closed state, three of the closest five inter-S6 contacts involve A653 interacting with F656, V659 and I655 (Table 1). The smallest distance across this interface occurs between A653 of one subunit and F656 of the adjacent subunit (average Cα–Cα/Cβ–Cβ distance = 5.2 Å) while in the open state this distance is 10.1 Å. In the closed-state model, A653 is buried at the centre of a hydrophobic pocket formed by the side chain of L650 from its own subunit and the side chains of F656, V659 and I655 from S6 of the adjacent subunit (Fig. 6*D*). The fact that this hydrophobic cluster forms the closest contacts between adjacent S6 helices, at the site of narrowest constriction in the vestibule, is suggestive that it plays an important role in stabilizing the structure of the closed-state tetramer.

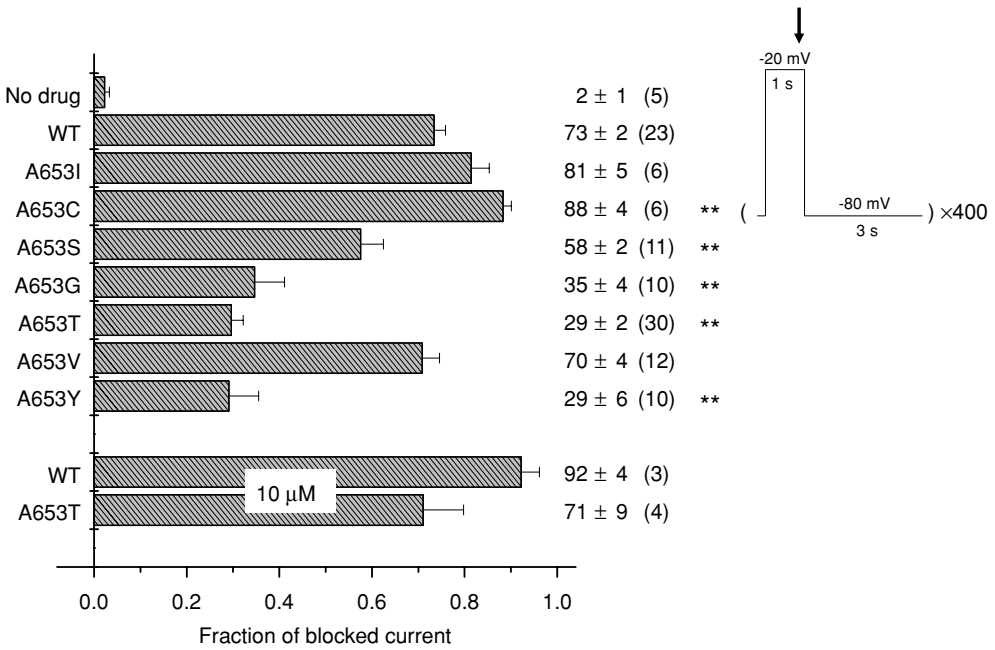

Figure 5. A specific subset of substitutions at position 653 affect dofetilide sensitivity of the HERG channel

Oocytes were repeatedly stepped from the resting potential to −20 mV for 1 s and then stepped back to −80 mV for 3 s (see inset) for the total of 26 min. Exposure to 1 μM dofetilide followed a 2 min drug-free period in which the current was allowed to stabilize. The fraction of blocked current measured at 26 min is shown as mean ± S.E.M. (n = 6–23), $^{**}P < 0.01$. The two lowest bars show the fraction of blocked current after application of 10 μM dofetilide, using the same protocol and the most drug-resistant variant, A653T. There was no direct correlation between drug sensitivity and gating characteristics.

Table 1. Closest WT S6–S6 helix contacts, as measured by the averaged Cα–Cα/Cβ–Cβ distances between residues of adjacent S6 helices in the closed-state model

Residue pairs	Average CαCβ inter-S6 distances (Å)
A653A–F656F	5.2
A653A–V659V	5.9
A661A–I663I	5.9
S654S–V659V	6.0
A653A–I655I	6.1

The observation that the A653 side chain is buried at the centre of this pocket implies a structural constraint that limits which modifications will be tolerated at position A653 in the closed state without perturbing the relative packing of adjacent S6 helices and/or F656 side chains in the vestibule. To test this hypothesis, structural perturbations introduced by A653 mutations were studied computationally. Consistent with this hypothesis, significant alterations of the packing arrangement were observed (see, e.g. Fig. 6*C*). For example, significant alteration of the F656 packing arrangement was observed in A653C/I/S/T/V and A653Y mutants, where there are gross steric clashes at the mutation sites that disallow the wild-type F656 rotamer conformations given the backbone geometry of our closed-state template. Such severe modifications in packing at this site would be expected to alter channel structure/function. Only A653G was arranged in a manner that allowed the F656 side chains to adopt a nearly WT conformation. However, due to the inherent flexibility that glycine introduces into the backbone (Magidovich & Yifrach, 2004; Ding *et al.* 2005), it is difficult to conclude precisely how this mutation might affect channel gating based on these models alone.

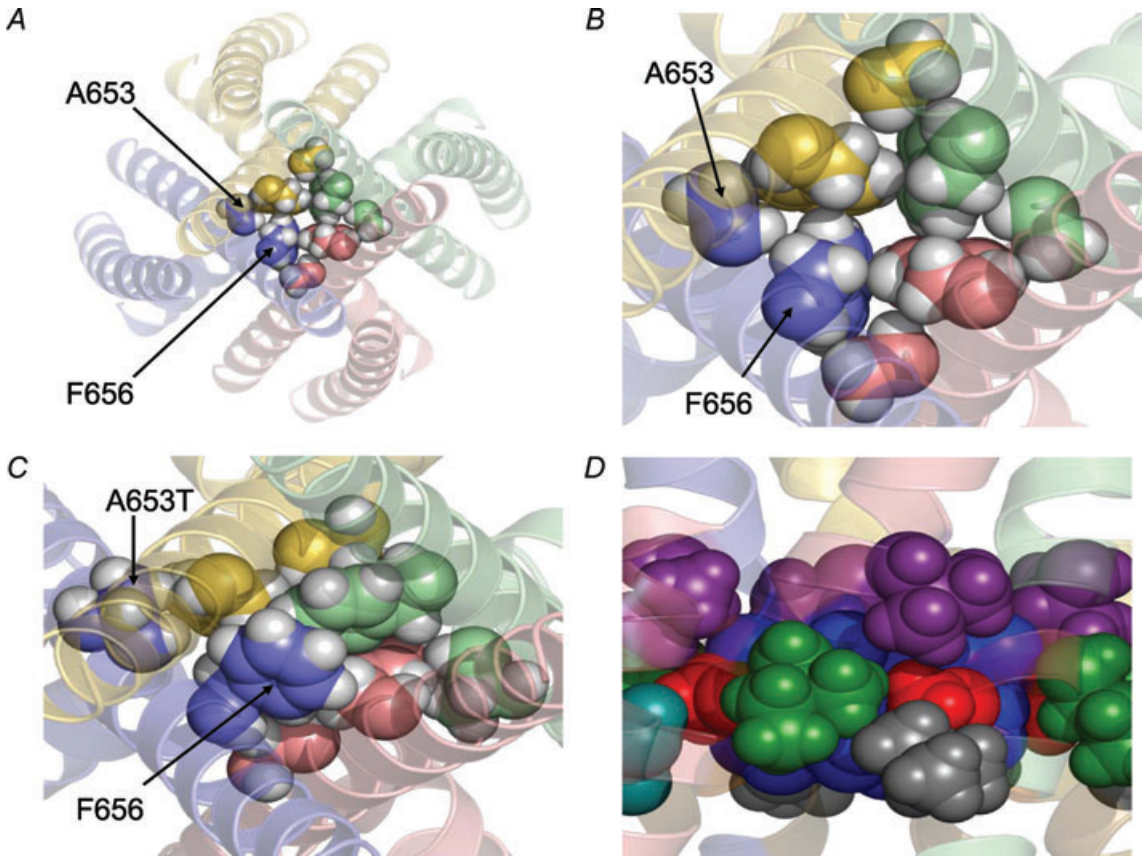

Figure 6. Molecular modelling of the closed and open states of the HERG channel at position 653
A, closed-state of wild-type HERG tetramer. *B*, close-up of the WT pore model in the closed state. *C*, close-up of the A653T mutant pore in the closed state. Side chain atoms of A653 and F656 are shown as spheres to highlight their interactions at the closest point of contact between adjacent S6 helices. Helices and residues are coloured by chain identity. *D*, hydrophobic pocket surrounding A653 residue. In the closed-state model, a hydrophobic cluster is formed by the side chains of A653 (red) and L650 (grey) from one subunit, and I655 (green), V659 (purple) and F656 (blue) from the adjacent subunit. The placement of A653 in a tight hydrophobic pocket may result in the observed intolerance for mutation. Residues 653 and 656 are indicated by arrows.

Discussion

This study focuses on the function of residue A653, located in the S6 transmembrane domain of HERG, which is highly conserved in the pore region of a variety of K^+ channels (Fig. 1). We find that amino acid substitutions at that position cause a spectrum of gating changes. All of the A653 variants caused leftward shifts in the $V_{1/2}$ of activation by as much as −51.3 mV. In addition, deactivation was greatly affected in all mutants, and in some cases (A653T/V/Y/G) the closed state could only be induced after stepping to very hyperpolarized potentials (below −100 mV) and holding for prolonged time periods. Use of the standard voltage-clamp protocol described in Fig. 2*A* revealed that A653S/G/Y/V and T show progressively greater defects in deactivation measured at −70 mV, as well as inward conduction at more negative potentials (see Fig. 2*A*) due to an accumulation of open channels. This indicates that these variants do not close in the physiologically relevant voltage range. A653I/C were least affected in that they deactivated at potentials negative to −60 mV (i.e. below the activation threshold), although they too displayed slowed deactivation kinetics. However, K^+ selectivity was not altered, and only two mutants, A653Y and A653G, displayed significantly altered voltage dependence of inactivation (Fig. 4*A*). The leftward shift in the activation curve and the slowed deactivation is consistent with a stabilization of the open state for all variants at position 653.

Mutations in related channels at positions homologous or close to HERG-A653 also result in constitutively open channels, or dramatic changes in channel opening/closing. For example, mutating the homologous alanine of the cyclic nucleotide-gated CNGA1 channel to a cysteine (A388C, Fig. 1), coupled with conjugation by 2−aminoethyl methane thiosulfonate hydrobromide (MTSEA), results in a channel that is constitutively open, even in the absence of ligand (Flynn & Zagotta, 2003). Another example is seen in a voltage-sensitive *Shaker*-KcsA chimera, where alanine substitution of the native G (G104A) at the position homologous to HERG-653 (see Fig. 1) alters the channel *I*–*V* relationship (Lu *et al.* 2001). The F380Y-substituted Ca^{2+}-activated BK_{Ca} channel causes a −150 mV shift in the $V_{1/2}$ of activation, yielding channels that remained open even in the absence of stimulation by Ca^{2+} (Lippiat *et al.* 2000). BK_{Ca}-F380 is located at a position analogous to HERG-Y652 (Fig. 1, grey shading), one amino acid upstream of HERG-A653. Finally, a mutation in the *Caenorhabditis elegans* HERG homologue, UNC103, at the analogous position A334T (see Fig. 1), causes an *in vivo* phenotype in *C. elegans* that is consistent with inappropriate K^+ channel hyperpolarization (Petersen *et al.* 2004). A similar phenotype is reported as a consequence of channel opening at hyperpolarized potentials in the homologous A to V mutation in the *C. elegans* egl-2 channel, and in the mouse eag channel (Weinshenker *et al.* 1999). While this manuscript was in preparation, Brown *et al.* reported functional findings that are compatible with our own, using substitution mutations of HERG-A653 (Brown *et al.* 2008). In addition, these authors reported that oxidation of A653C HERG alters the gating of the mutant channel, although the effect was not reversible upon addition of DTT, indicating that disulfide bonds between adjacent 653C residues are unlikely.

Very recently, a study of cysteine substitutions at various positions throughout the HERG S6 domain (but not including A653) described slowed deactivation and negative shifts in the $V_{1/2}$ of activation in response to some of the variants studied (Wynia-Smith *et al.* 2008). The S654C mutation, affecting the residue immediately downstream, resulted in only minor gating changes, further highlighting the unique importance of A653. This observation is consistent with our model, where S654 is located on the outer face of S6 pointing away from the adjacent subunit and toward the S5 helix of the same subunit.

Two bulky aromatic residues, Y652 and F656 (Fig. 1, grey shading) that are bracketing A653, are crucial for high affinity drug binding to several chemically divergent compounds, including the class III anti-arrhythmic agent dofetilide (Spector *et al.* 1996; Fernandez *et al.* 2004; Mitcheson *et al.* 2005; Kamiya *et al.* 2006). Prior studies have correlated specific gated states and drug sensitivity of HERG (Carmeliet, 1992; Snyders & Chaudhary, 1996; Spector *et al.* 1996; Kiehn *et al.* 1996; Herzberg *et al.* 1998; Ficker *et al.* 1998, 2001; Mitcheson *et al.* 2000; Tsujimae *et al.* 2004). Sanguinetti's group described the drug sensitivity and gating phenotype of HERG variants in which the Y and F residues are substituted using a number of diverse amino acids (Chen *et al.* 2002; Fernandez *et al.* 2004). While the substitutions disrupted channel closure and drug sensitivity to varying degrees, the two effects did not correlate well and were not closely related. Similarly, our results (Fig. 5) indicated no consistent correlation between drug sensitivity and the gating defects. We therefore conclude that affinity to dofetilide in some of the variants was altered due to the effect of A653 on the drug binding pocket, rather than deactivation gating. The gating characteristics of HERG variants at position 656 have been described (Mitcheson *et al.* 2000; Lees-Miller *et al.* 2000; Fernandez *et al.* 2004); they do not show drastically altered deactivation or defects in closing.

We constructed computational models of the HERG S5 to S6 domains in the closed and open states via homology modelling using KcsA (PDB entry: 1K4C) as the template for the closed state and KvAP (PDB entry: 1ORQ) as the template for the open state structure. The resulting models are similar (root mean square deviation ∼3.0 Å) to

previously published models (Masetti *et al.* 2007) built using a united-atom molecular dynamics approach. Analysis of the homology models indicates that HERG-A653 plays an important role in stabilizing the closed-state conformation through interactions with HERG-F656, V659 and I655 of the neighbouring subunit. The packing of the A653 side chain between the side chains of F656, V659 and I655 appears to form a hydrophobic cluster (Fig. 6*D*) that constitutes the closest packing between adjacent S6 helices as well as the narrowest point within the channel cavity itself. Indeed, Brown *et al.* recently showed (Brown *et al.* 2008) that mutating residue 656 prevents the hyperpolarizing shift in $V_{1/2}$ of channel activation observed with A653V, thus demonstrating a functional interaction between residues 656 and 653.

Based on the crystal structure of MthK, Jiang *et al.* (2002) suggested an important role for MthK-A88 (homologous to HERG-A653, Fig. 1), as the narrowest point of the open intracellular cavity in permitting ion flow. Fernandez *et al.* (2004) suggested F656 as the defining constriction point in the closed-state pore. Our model appears to unify these two prior observations by implicating the interaction between A653 and F656, among others, as being a key stabilizing factor in the S6–S6 packing interface. The details of the S6–S6 packing interface necessarily define the constriction point of the vestibule in the context of the tetramer. Our model therefore suggests that A653 is a key determinant of the tertiary arrangement of S6 helices in the closed-state tetramer, and is therefore central to defining ion channel gating.

The current phenotypes of the seven variants we tested did not permit a straightforward correlation between the hydrophobicity or size of individual amino acid substitutions and effects on deactivation gating, suggesting that the closed state is determined by more than one variable at that position. At present, we can only speculate about reasons why certain substitutions at position 653 prevent channel closing at physiologically relevant potentials, whereas others do not. (1) Glycine in the A653G variant may confer extra flexibility on the S6 helices allowing for a hinged bending and opening ('leaking') of the channel (Magidovich & Yifrach, 2004; Ding *et al.* 2005). (2) Our model suggests that the large residue introduced with the A653Y or A653T mutation would not fit the narrowest point of the cavity, and would destabilize the closed state, as well as perhaps stabilize the open state through interaction with Y652 on the same subunit in the case of A653Y. (3) Compared to A, V and T have an extra methyl or hydroxyl group that may disrupt interactions with the S6 backbone and F656 side chains in the closed state, or may otherwise stabilize the open state. (4) A653I may have relatively minor overall effects because isoleucine has a methyl group that may be engaged, despite the fact that its branch chain is relatively large. The packing of the helices and function of substituted amino acids will be the subject of future studies.

In summary, the gating effects of the A653 variants described in this study, in combination with computational modelling results, demonstrate the critical involvement of this residue in the K^+ channel closure. Depending on the individual characteristics of the amino acid occupying this position, channel closing at physiological potentials is impaired to varying degrees. The residue appears to be located at the narrowest point of the inner cavity and may contribute to the stabilization of an inter-subunit S6 helix–helix packing interaction. Our data, when considered in the context of published data regarding residues at analogous positions in other K^+ channels, suggest a close functional relationship between A653 and a voltage-dependent channel closure mechanism that creates outward rectification and is evolutionarily conserved. We find that substitutions at this position do not support channel closing at physiologically relevant membrane potentials, and that the conservation of alanine is therefore critical for closing in the native channel.

References

Adams SV & DeFelice LJ (2003). Ionic currents in the human serotonin transporter reveal inconsistencies in the alternating access hypothesis. *Biophys J* **85**, 1548–1559.

Armoundas AA, Wu R, Juang G, Marban E & Tomaselli GF (2001). Electrical and structural remodeling of the failing ventricle. *Pharmacol Ther* **92**, 213–230.

Armstrong CM (2003). Voltage-gated K channels. *Sci STKE* **188**, re10.

Brown S, Sonntag DP & Sanguinetti MC (2008). A highly conserved alanine in the S6 domain of the hERG1 K^+ channel is required for normal gating. *Cell Physiol Biochem* **22**, 601–610.

Carmeliet E (1992). Voltage- and time-dependent block of the delayed K^+ current in cardiac myocytes by dofetilide. *J Pharmacol Exp Ther* **262**, 809–817.

Chen J, Mitcheson JS, Tristani-Firouzi M, Lin M & Sanguinetti MC (2001). The S4-S5 linker couples voltage sensing and activation of pacemaker channels. *Proc Natl Acad Sci U S A* **98**, 11277–11282.

Chen J, Seebohm G & Sanguinetti MC (2002). Position of aromatic residues in the S6 domain, not inactivation, dictates cisapride sensitivity of HERG and eag potassium channels. *Proc Natl Acad Sci U S A* **99**, 12461–12466.

Choy A-M, Kuperschmidt S, Lang CC, Pierson RN & Roden DM (1996). Regional expression of HERG and KvLQT1 in heart failure. *Circulation* **94**, 1–164.

Curran ME, Splawski I, Timothy KW, Vincent GM, Green ED & Keating MT (1995). A molecular basis for cardiac arrhythmia: HERG mutations cause long QT syndrome. *Cell* **80**, 795–803.

Decher N, Chen J & Sanguinetti MC (2004). Voltage-dependent gating of hyperpolarization-activated, cyclic nucleotide-gated pacemaker channels: molecular coupling between the S4-S5 and C-linkers. *J Biol Chem* **279**, 13859–13865.

Ding S, Ingleby L, Ahern CA & Horn R (2005). Investigating the putative glycine hinge in *Shaker* potassium channel. *J Gen Physiol* **126**, 213–226.

Doyle DA, Morais Cabral J, Pfuetzner RA, Kuo A, Gulbis JM, Cohen SL, Chait BT & MacKinnon R (1998). The structure of the potassium channel: molecular basis of K^+ conduction and selectivity. *Science* **280**, 69–77.

Etheridge S, Compton S, Tristani-Firouzi M & Mason J (2003). A new oral therapy for long QT syndrome: long-term oral potassium improves repolarization in patients with HERG mutations. *J Am Coll Cardiol* **42**, 1777–1782.

Fernandez D, Ghanta A, Kauffman G & Sanguinetti MC (2004). Physicochemical features of the HERG channel drug binding site. *J Biol Chem* **279**, 10120–10127.

Ficker E, Jarolimek W & Brown AM (2001). Molecular determinants of inactivation and dofetilide block in *ether a-go-go* (EAG) channels and EAG-related K^+ channels. *Mol Pharmacol* **60**, 1343–1348.

Ficker E, Jarolimek W, Kiehn J, Baumann A & Brown AM (1998). Molecular determinants of dofetilide block of HERG K^+ channels. *Circ Res* **82**, 386–395.

Flynn GE & Zagotta WN (2003). A cysteine scan of the inner vestibule of cyclic nucleotide-gated channels reveals architecture and rearrangement of the pore. *J Gen Physiol* **121**, 563–583.

Herzberg IM, Trudeau MC & Robertson GA (1998). Transfer of rapid inactivation and sensitivity to the class III antiarrhythmic drug E-4031 from HERG to M-eag channels. *J Physiol* **511**, 3–14.

Jiang Y, Lee A, Chen J, Cadene M, Chait BT & MacKinnon R (2002). The open pore conformation of potassium channels. *Nature* **417**, 523–526.

Jiang Y, Lee A, Chen J, Ruta V, Cadene M, Chait BT & MacKinnon R (2003). X-ray structure of a voltage-dependent K^+ channel. *Nature* **423**, 33–41.

Kamiya K, Niwa R, Mitcheson S & Sanguinetti M (2006). Molecular determinants of hERG channel block. *Mol Pharmacol* **69**, 1709–1716.

Kiehn J, Lacerda AE, Wible B & Brown AM (1996). Molecular physiology and pharmacology of HERG. Single-channel currents and block by dofetilide. *Circulation* **94**, 2572–2579.

Kupershmidt S, Yang IC, Hayashi K, Wei J, Chanthaphaychith S, Petersen CI, Johns DC, George Jr AL, Roden DM & Balser JR (2003). I_{Kr} drug response is modulated by *KCR1* in transfected cardiac and noncardiac cell lines. *FASEB J* **17**, 2263–2265.

Lees-Miller JP, Duan Y, Teng GQ & Duff HJ (2000). Molecular determinant of high-affinity dofetilide binding to HERG1 expressed in *Xenopus* oocytes: involvement of S6 sites. *Mol Pharmacol* **57**, 367–374.

Lippiat JD, Standen NB & Davies NW (2000). A residue in the intracellular vestibule of the pore is critical for gating and permeation in Ca^{2+}-activated K^+ (BKCa) channels. *J Physiol* **529**, 131–138.

Long SB, Campbell EB & MacKinnon R (2005*a*). Crystal structure of a mammalian voltage-dependent *Shaker* family K^+ channel. *Science* **309**, 897–903.

Long SB, Campbell EB & MacKinnon R (2005*b*). Voltage sensor of Kv1.2: structural basis of electromechanical coupling. *Science* **309**, 903–908.

Lu Z, Klem AM & Ramu Y (2001). Ion conduction pore is conserved among potassium channels. *Nature* **413**, 809–813.

Lu Z, Klem AM & Ramu Y (2002). Coupling between voltage sensors and activation gate in voltage-gated K^+ channels. *J Gen Physiol* **120**, 663–676.

Magidovich E & Yifrach O (2004). Conserved gating hinge in ligand- and voltage-dependent K^+ channels. *Biochemistry* **43**, 13242–13247.

Masetti M, Cavalli A & Recanatini M (2007). Modeling the hERG potassium channel in a phospholipid bilayer: Molecular dynamics and drug docking studies. *J Comput Chem* **29**, 795–808.

Mitcheson J, Perry M, Stansfeld P, Sanguinetti M, Witchel H & Hancox J (2005). Structural determinants for high-affinity block of hERG potassium channels. *Novartis Found Symp* **266**, 136–150.

Mitcheson JS, Chen J, Lin M, Culberson C & Sanguinetti MC (2000). A structural basis for drug-induced long QT syndrome. *Proc Natl Acad Sci U S A* **97**, 12329–12333.

Petersen CI, McFarland TR, Stepanovic SZ, Yang P, Reiner DJ, Hayashi K, George AL, Roden DM, Thomas JH & Balser JR (2004). *In vivo* identification of genes that modify ether-a-go-go-related gene activity in *Caenorhabditis elegans* may also affect human cardiac arrhythmia. *Proc Natl Acad Sci U S A* **101**, 11773–11778.

Pettersen EF, Goddard TD, Huang CC, Couch GS, Greenblatt DM, Meng EC & Ferrin TE (2004). UCSF Chimera – a visualization system for exploratory research and analysis. *J Comput Chem* **25**, 1605–1612.

Pischalnikova AV & Sokolova OS (2009). The domain and conformational organization in potassium voltage-gated ion channels. *J Neuroimmune Pharmacol* **4**, 71–82

Roden DM & Spooner PM (1999). Inherited long QT syndromes: a paradigm for understanding arrhythmogenesis. *J Cardiovasc Electrophysiol* **10**, 1664–1683.

Roden DM & Viswanathan PC (2005). Genetics of acquired long QT syndrome. *J Clin Invest* **115**, 2025–2032.

Roden DM, Balser JR, George AL Jr & Anderson ME (2002). Cardiac ion channels. *Annu Rev Physiol* **64**, 431–475.

Rohl CA, Strauss CE, Chivian D & Baker D (2004). Modeling structurally variable regions in homologous proteins with rosetta. *Proteins* **55**, 656–677.

Sanguinetti MC, Jiang C, Curran ME & Keating MT (1995). A mechanistic link between an inherited and an acquired cardiac arrhythmia: *HERG* encodes the I_{Kr} potassium channel. *Cell* **81**, 299–307.

Smith JA, Vanoye CG, George AL Jr, Meiler J & Sanders CR (2007). Structural models for the KCNQ1 voltage-gated potassium channel. *Biochemistry* **46**, 14141–14152.

Smith PL, Baukrowitz T & Yellen G (1996). The inward rectification mechanism of the HERG cardiac potassium channel. *Nature* **379**, 833–836.

Snyders DJ & Chaudhary A (1996). High affinity open channel block by dofetilide of HERG expressed in a human cell line. *Mol Pharmacol* **49**, 949–955.

Spector PS, Curran ME, Keating MT & Sanguinetti MC (1996). Class III antiarrhythmic drugs block HERG, a human cardiac delayed rectifier K^+ channel. Open-channel block by methanesulfonanilides. *Circ Res* **78**, 499–503.

Tristani-Firouzi M, Chen J & Sanguinetti MC (2002). Interactions between S4-S5 linker and S6 transmembrane domain modulate gating of HERG K^+ channels. *J Biol Chem* **277**, 18994–19000.

Trudeau M, Warmke J, Ganetzky B & Robertson G (1995). HERG, a human inward rectifier in the voltage-gated potassium channel family. *Science* **269**, 92–95.

Tseng GN (2001). I_{Kr}: the hERG channel. *J Mol Cell Cardiol* **33**, 835–849.

Tsujimae K, Suzuki S, Yamada M & Kurachi Y (2004). Comparison of kinetic properties of quinidine and dofetilide block of HERG channels. *Eur J Pharmacol* **493**, 29–40.

Weinshenker D, Wei A, Salkoff L & Thomas JH (1999). Block of an ether-a-go-go-like K^+ channel by imipramine rescues egl−2 excitation defects in *Caenorhabditis elegans*. *J Neurosci* **19**, 9831–9840.

Wynia-Smith SL, Gillian-Daniel AL, Satyshur KA & Robertson GA (2008). hERG gating microdomains defined by S6 mutagenesis and molecular modeling. *J Gen Physiol* **132**, 507–520.

Zhou Y, Morais-Cabral JH, Kaufman A & MacKinnon R (2001). Chemistry of ion coordination and hydration revealed by a K^+ channel–Fab complex at 2.0 Å resolution. *Nature* **414**, 43–48.

Zou A, Curran ME, Keating MT & Sanguinetti MC (1997). Single HERG delayed rectifier K^+ channels expressed in *Xenopus* oocytes. *Am J Physiol Heart Circ Physiol* **272**, H1309–H1314.

Author contributions

Svetlana Stepanovic was responsible for collecting data, designing experiments, analysing data, and drafting the manuscript. Franck Potet was responsible for collecting data, designing experiments, and analysing data. Christina Petersen was involved in the conception of the initial work and in drafting the experiments. Jarrod Smith was involved in the design and execution of the molecular modelling experiments and for revising the article. Jens Meiler was responsible for the analysis and conception of the molecular modelling experiments and for revising the article. Jeffrey Balser was involved in revising the article critically for important intellectual content. Sabina Kupershmidt was involved in drafting, writing, editing and revising the article for intellectual content and in coordinating the groups of investigators involved with the work. All of the work was done at Vanderbilt University, Nashville, TN, USA.

Acknowledgements

We wish to thank Dr Louis DeFelice (Vanderbilt University) for kindly supplying us with *Xenopus* oocytes. We thank Dr Prakash Viswanathan for critical reading of the manuscript. This study was supported by funding from the National Heart, Lung and Blood Institute P01 HL46681 (J.R.B.), by the James Tayloe Gwathmey fund (J.R.B.) and by the National Institute of General Medical Sciences R01-GM080403 (J.M.).